

First-principles investigation of effect of pressure on BaFe₂As₂

Wenhui Xie, Mingli Bao, Zhenjie Zhao

*Department of Physics, East China Normal University, Shanghai, 200062, China and
Engineering Research Center for Nanophotonics and Advanced Instrument,
East China Normal University, Shanghai, 200062, China*

Bang-Gui Liu

*Institute of Physics, Chinese Academy of Sciences, Beijing 100190, China
(Dated: November 3, 2018)*

On experimental side, BaFe₂As₂ without doping has been made superconducting by applying appropriate pressure (2-6 GPa). Here, we use a full-potential linear augmented plane wave method within the density-functional theory to investigate the effect of pressure on its crystal structure, magnetic order, and electronic structure. Our calculations show that the striped antiferromagnetic order observed in experiment is stable against pressure up to 13 GPa. Calculated antiferromagnetic lattice parameters are in good agreements with experimental data, while calculations with nonmagnetic state underestimate Fe-As bond length and c-axis lattice constant. The effects of pressure on crystal structure and electronic structure are investigated for both the antiferromagnetic state and the nonmagnetic one. We find that the compressibility of the antiferromagnetic state is quite isotropic up to about 6.4 GPa. With increasing pressure, the FeAs₄ tetrahedra is hardly distorted. We observe a transition of Fermi surface topology in the striped antiferromagnetic state when the compression of volume is beyond 8% (or pressure 6 GPa), which corresponds to a large change of c/a ratio. These first-principles results should be useful to understanding the antiferromagnetism and electronic states in the FeAs-based materials, and may have some useful implications to the superconductivity.

PACS numbers:

I. INTRODUCTION

The discovery of high temperature superconductivity in iron-pnictide materials¹ has attracted widespread interest in elucidating the superconductivity mechanism and searching for new high- T_c materials^{2,3,4}. The highest critical temperature (T_c) observed in the RFeAsO series compounds (R= La-Gd) is up to 55 K with electron doping^{5,6}. Recently, superconductivity was discovered in the AFe₂As₂ materials (A = Ca, Ba, Sr) which have similar FeAs layers. It has been reported that the transition temperature can be as high as 38 K for (K,Ba)Fe₂As₂ and (K,Sr)Fe₂As₂^{7,8}. All of these compounds show an antiferromagnetic order and a structural transition with similar ordering temperatures⁹. Although the superconductivity mechanism is not yet known up to now, the phonon mediated pairing seems to be ruled out¹⁰. The fact that antiferromagnetic spin fluctuations coexist with superconductivity indicates that the nature of superconductivity should be complex and unconventional in the FeAs-based compounds^{3,4,11}, like that of the cuprate high- T_c superconductors.

Stoichiometric BaFe₂As₂ is not superconductor but an antiferromagnet^{12,13}. Superconductivity can be achieved by either electron or hole doping. In hole doped superconducting (K,Ba)Fe₂As₂, $T_c=38$ K has been obtained by replacing 40% Ba by K⁷. So that BaFe₂As₂ is a typical parent compound of the high temperature iron-arsenides superconductors. In addition, recent experiments confirmed that BaFe₂As₂ without doping becomes superconducting under high pressure¹⁴. The pressure inducing

superconductivity was also observed in the same group compounds SrFe₂As₂¹⁴ and CaFe₂As₂¹⁵. It is very interesting to investigate the properties of AFe₂As₂ materials under high pressure.

In this paper we use full-potential augmented-plane-wave method based on the density-functional theory to investigate pressure effect on the crystal structure, magnetism and electronic structure of BaFe₂As₂. The reason we concentrate on BaFe₂As₂ to investigate the pressure effect is that its superconductivity, in a wide pressure range (between 2-6 GPa) and the highest T_c up to 28 K, is more robust than that of the Sr and Ca compounds¹⁴. At first, we analyze the effects of different magnetic orders on the equilibrium lattice parameters and corresponding electronic structures. Our calculation indicates that the striped antiferromagnetic state is the ground state, its calculated crystal structure and lattice constants are consistent with experimental data. With increasing pressure, there is a topological transition of Fermi surfaces in the striped antiferromagnetic state approximately at 6 GPa. This Fermi surface transition is possibly related to the structural transition and consistent with the loss of superconductivity at the pressure. These full-potential DFT results should be helpful to understand the pressure-induced properties of BaFe₂As₂¹¹.

The remaining part of this paper is organized as follows. In next section, we describe our computational method and parameters. In section III, we analyze the crystal structure, magnetic orders and electronic structures under ambient pressure. In Section IV, we present pressure-driven changes of the crystal structure, mag-

netic order, and electronic structures. In section V, we compare our calculated results with known experimental results. Finally, we give our conclusion in section VI.

II. COMPUTATIONAL METHOD

The present calculations are performed by using an *ab initio* all-electron full-potential linearized augmented plane wave (FLAPW) method based on the density-functional theory, as implemented in WIEN2K code¹⁶. Both local density approximation (LDA)¹⁷ and generalized gradient approximation (GGA)¹⁸ are used in our calculations. The atomic sphere radii of 2.4, 2.0, and 1.9 atomic unit are used for Ba, Fe and As, respectively. The self-consistent calculations are considered to be converged only when the integrated charge difference between input and output charge density is less than 0.0001. The internal parameter z_{As} , describing the As position, is relaxed until the force per atom is smaller than 1mRy/a.u. We use 500 k -points for Brillouin-zone integrations in the antiferromagnetic calculations, and at least 1500 k -points in the nonmagnetic calculation.

BaFe₂As₂ has ThCr₂Si₂ type body centered tetragonal structure ($I4/mmm$) with lattice parameters $a = 3.9625 \text{ \AA}$ and $b = 13.0168 \text{ \AA}$ at room temperature. The FeAs layers are stacked so that the As atoms face each other and the Ba atoms sit in the resulting 8-fold coordinated square prismatic sites between them. At 140 K, it undergoes a structural phase transition from tetragonal to orthorhombic structure ($Fmmm$) with lattice constants $a = 5.6146 \text{ \AA}$, $b = 5.5742 \text{ \AA}$, and $c = 12.9453 \text{ \AA}$ (at 20K), accompanied by a magnetic phase transition from a Pauli paramagnetism to an antiferromagnetic order. Neutron scattering experiments have shown that the magnetic moments are aligned ferromagnetically along b -axis but antiferromagnetically along a -axis and c -axis^{13,19}, the named striped antiferromagnetic order state (AF1). We also calculated checkerboard antiferromagnetic order state (AF2), in which magnetic moment of nearest-neighbor Fe are antiferromagnetic order while magnetic moment of next nearest-neighbor are ferromagnetic order. In all the calculations, we keep b/a ratio in term of the experimental value because we have found that the changing of b/a has tiny influence on the total energy and electronic structure.

III. ANALYSIS OF AMBIENT-PRESSURE PROPERTIES

As a starting point, we took the experimental lattice parameters of tetragonal paramagnetic state and the striped antiferromagnetic state of BaFe₂As₂, and relaxed the internal coordinate of As by LDA calculation with generalized gradient approximation (GGA). For nonmagnetic state, we found that relaxed internal parameter of $z_{\text{As}} = 0.3448$ is much lower than the experimental value of

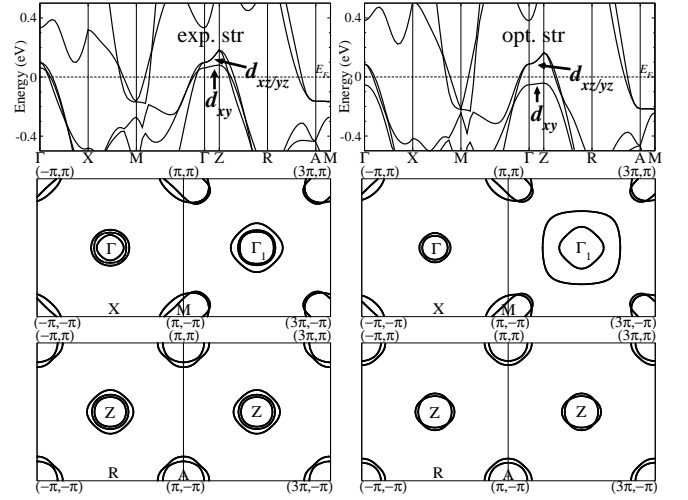


FIG. 1: Band structure (top two panels) and Fermi surface sections (the other four panels) of BaFe₂As₂ of experimental lattice constant with experimental As coordinates z_{As} (left column, labelled as exp. str) and with *ab initio* optimized value (right column, labelled as opt. str). The middle panels show the Fermi surface sections extended to the second Brillouin zone in the k_x direction for the $k_z = 0$ plane, and the bottom panels show those for the $k_z = \pi/c$ plane.

$z_{\text{As}} = 0.3545$. While for the striped antiferromagnetic order, we arranged the direction of iron magnetic moment in terms of experimental observation¹⁹, and got a value of $z_{\text{As}} = 0.3515$, which is in better agreement with experimental data of $z_{\text{As}} = 0.3538$ ¹⁹. Other antiferromagnetic settings with optimized lattice parameters cause smaller z_{As} value, but are better than nonmagnetic result. Calculated magnetic moment of iron inside muffin tin sphere is $1.86\mu_B$, almost twice larger than the value of $0.8\mu_B$ measured by neutron scattering experiment¹⁹.

It turns out that the band character of BaFe₂As₂ is similar to that of LaFeAsO¹⁰, except that La f and O p states are missing in BaFe₂As₂ compound. The band splitting of d_{3z^2-1} states is also significantly weaker in BaFe₂As₂ than in LaFeAsO, which indicates that inter-layer bonding through the Ba layer of BaFe₂As₂ is weaker than the LaO layers of LaFeAsO. Since there have been many reports on the electronic structures^{21,22,23,24}, we show only the bands near Fermi level to manifest the key parts. The band structure and Fermi surfaces of tetragonal phase are illustrated in Fig. 1 for both experimental and optimized structures.

Fermi surfaces of both experimental and optimized structures have a doubly-degenerated electron pocket centered at the M point. These sheets have a dominant d_{xz}, d_{yz} character, only a little component of d_{xy} character. Around Γ point, there is significant difference. For optimized structure, Fermi surfaces comprise a doubly-degenerated cylindrical hole pocket centered at the Γ point, mainly consisting of $d_{xz/yz}$ character and little mixture of $d_{x^2-y^2}$ and d_{3z^2-1} . While for experimental structure, another new cylindrical hole sheet, mainly

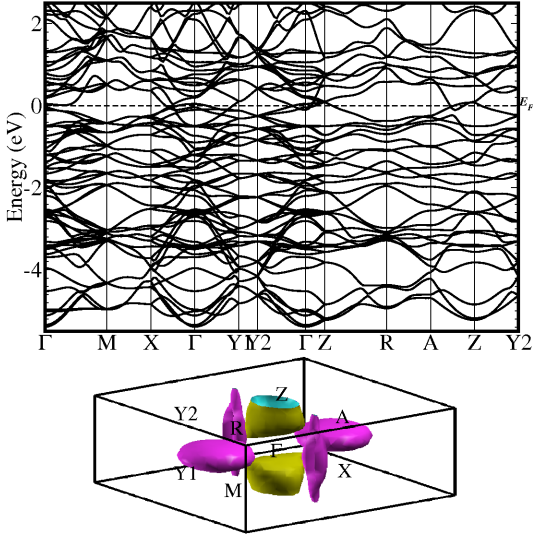


FIG. 2: (color online). Band structures and Fermi surfaces of the striped antiferromagnetic state with experimental lattice. Here, we use a orthogonal lattice and show Fermi surfaces on a conventional orthogonal BZ. The choice of BZ does not influence our main discussions and results, but is better to guide for eyes.

d_{xy} character, inserted to the two hole sheets. Those sheets have more two-dimensional character. Compared to the observation of APRES experiment²⁰, the calculated results using the experimental lattice parameters are in better agreement with ARPES data. Furthermore, in comparison with other calculated results^{21,22,23,24}, we would find that whether d_{xy} bands cross Fermi level or not, it is sensitive to z_{As} , which is similar to the results discussed in LaFeAsO system^{11,23}.

Furthermore, it is found that the band width of the d_{xy} bands changes little, but they shift downwards by about 0.2 eV in comparison to the $d_{xz/yz}$ bands. This fact indicates that the tiny change of As position has a significant effect on the crystal splitting between d_{xy} and $d_{xz/yz}$ orbital bands. Since there is direct d_{xy} coupling between the two Fe atoms, the d_{xy} bands are not sensitive to the change of the z_{As} position and are more likely affected by the Fe-Fe distance, while $d_{xz/yz}$ orbital are likely coupled with As p orbital states (mainly p_x and p_y), the $d_{xz/yz}$ bands have stronger k_z dispersion than the d_{xy} bands and the corresponding Fermi surfaces have more three-dimensional (3-D) character, which change more distinctively as the Fe-As bond length is shortened. The discrepancy of Fe-As bond length between *ab initio* calculations and experimental data, which is induced by the magnetism, is a common feature of superconducting iron-pnictide family. This is because the iron-pnictide materials is in proximity to a quantum critical point, results in a strong spin fluctuations¹¹.

In Fig. 2, we show the band structures and Fermi surfaces of the striped antiferromagnetic state with experimental lattice constants. In Fig. 3, we show the

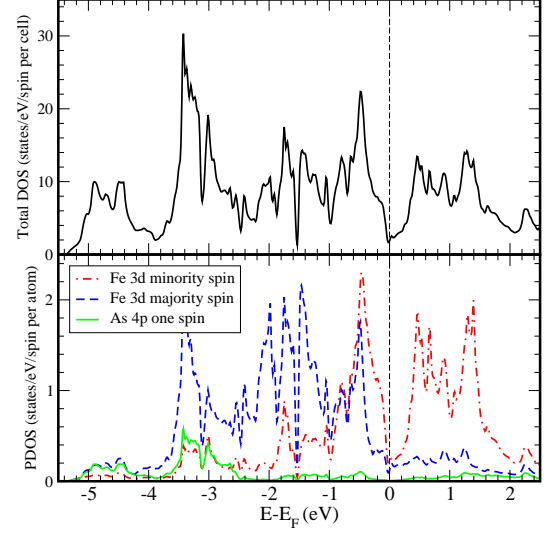


FIG. 3: (color online). Top panel: total DOS for the striped antiferromagnetic state. Bottom panel: spin resolved Fe 3d DOS, showing majority (blue) and minority (red), and the As 4p DOS (green).

total density of states (DOS) and the partial DOS of Fe 3d and As 4p states in different boxes. The bands from ~ -6 eV to -2 eV are mainly from As p states. The Fe d bands range from -2 eV to $+3$ eV, being above As p states. Around -3 eV, there is significant hybridization between the Fe d states and As p states. The band character around the Fermi level is dominated by d orbital. Due to the striped antiferromagnetic order, a pseudo-gap is opened near the Fermi level around Γ point. In Fig. 2, we could find the shape of Fermi surfaces is not regular due to the complex d bands dispersion around the Fermi level induced by antiferromagnetic interaction. There are hole-type Fermi surfaces around Z point (yellow), two slender electron-type Fermi surfaces parallel to Γ -Z line located at k_x direction, and two irregular electron-type Fermi surfaces located at Γ -Y1 line (pink) which are separated and confined in one quarter of BZ. They are mainly of d_{xy} , d_{xz} and d_{yz} characters, with some mixing of $d_{x^2-y^2}$ and d_{3z^2-1} characters.

Compared to the quasi-two-dimensional Fermi surfaces of the striped antiferromagnetic LaOFeAs⁴, the Fermi surfaces of BaFe₂As₂ have distinct three-dimensional topology. The effect of the orthorhombic lattice distortion on the electronic band structure as well as the Fe moments is very weak. The inter-layer spin interaction is antiferromagnetic because our total energy calculations show that the ferromagnetic order state is higher by about 2.6 meV in total energy per Fe atom. The inter-layer spin coupling constant is estimated to be $J_{\perp} = 0.8$ meV. The most stable striped antiferromagnetic order state with a magnetic moment $1.86\mu_B$ is energy lower 124 meV per Fe atom than the nonmagnetic state, while the checkerboard antiferromagnetic order state with a mag-

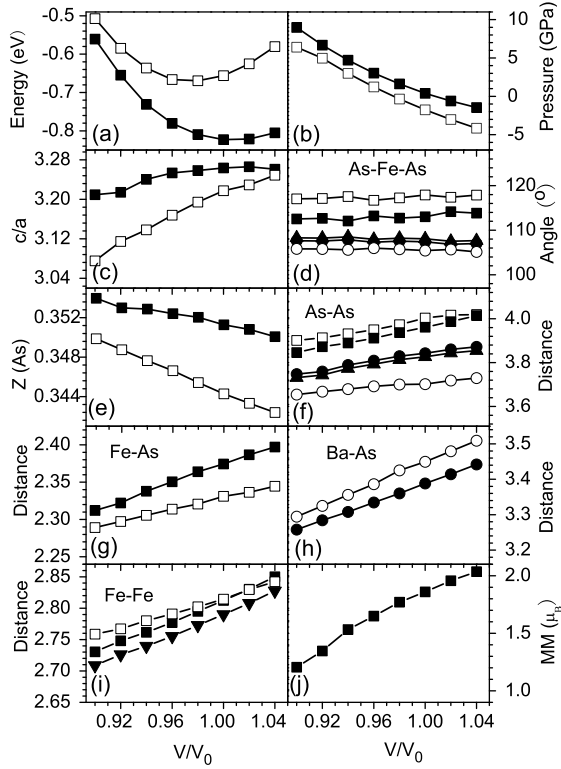


FIG. 4: Calculated values of total energy (a), pressure (b), c/a ratio (c), As-Fe-As angle (d), z_{As} (e), Fe-As bond length (f), As-As bond length (g), Ba-As bond length (h), Fe-Fe bond length (i), magnetic moment of iron (j) as functions of volume (V_0 is the experimental volume of the antiferromagnetic state per formula unit, which is about 0.2% smaller than the experimental value of nonmagnetic state). Filled symbols indicate the striped antiferromagnetic results, and open symbols nonmagnetic ones. For the As-As distance and As-Fe-As angle, due to the orthorhombic distortion, antiferromagnetic state has three values while nonmagnetic state has only two.

netic moment $1.63\mu_B$ is only 54 meV energy lower. By mapping to a simple Heisenberg model only including the 1st and 2nd neighbor exchange couplings, we could estimate the coupling constants: $J_{1a} = 28.2$ meV, $J_{1b} = 27.3$ meV and $J_2 = 17.4$ meV. The tiny difference between the coupling constants J_{1a} (along a -axis) and J_{1b} (along b -axis) indicates that exchange coupling of BaFe_2As_2 is not so anisotropic.

IV. EFFECT OF PRESSURE ON CRYSTAL STRUCTURE, MAGNETIC ORDER, AND ELECTRONIC STRUCTURE

Now we investigate the effect of pressure on the crystal structure and electronic structure of BaFe_2As_2 . We compress crystal volume up to 18%, corresponding to pressure of 18 GPa (about 180 kbar). We relax the internal parameters z_{As} and c/a ratio (keeping b/a ratio of orthorhombic structure in term of the experimental

TABLE I: Calculated equilibrium lattice constant (in unit of Å) with internal parameter (z_{As}) of BaFe_2As_2 obtained from the fully optimized nonmagnetic (NM) and striped antiferromagnetic (AF1) calculations.

	exp.(NM)	exp.(AF1)	cal.(NM)	cal.(AF1)
Spacegroup	$I4/mmm$	$Fmmm$	$I4/mmm$	$Fmmm$
a (Å)	3.9625	5.6146	3.9591	5.6378
b (Å)		5.5742		5.5931
c (Å)	13.0168	12.9453	12.6210	12.9624
z_{As}	0.3545	0.3538	0.3448	0.3512
$d(\text{As-Fe})$ (Å)	2.403	2.392	2.3330	2.3789

value) of all structures at intervals of 2% volume compression. We subsequently fit the $E \sim V$ curves to a Birch-Murnaghan equation-of-state, to obtain the equilibrium volume V_0 and the bulk modulus B_0 for each system. The magnetic moment decreases with increasing pressure, which results in possible small change of b/a , but this change hardly influences other structural parameters such as z_{As} and the electronic structure. Therefore, it is reasonable to keep b/a in our magnetic calculations.

The theoretical lattice constants and internal parameters obtained by the complete optimization are listed in Table I. As expected, nonmagnetic calculations underestimate c/a ratio because As atom is more close to Fe layers. We could find that nonmagnetic calculation roughly predict the in-plane Fe-Fe bonding correctly, but shorten out-of-plane Fe-As bond length, therefore As atom is more close to iron layer, resulting in a small z_{As} . While the calculated lattice parameters of the striped antiferromagnetic state are in better agreement with experimental data. Furthermore, the striped antiferromagnetic calculation could also describe out-of-plane Ba-As and As-As bond better.

In Fig. 4, we show the dependence of structural parameters on the compression of volume for both nonmagnetic and striped antiferromagnetic states. The total energy, pressure, the bond length, bond angle, and the magnetic moment of iron are illustrated as functions of the compression of volume. The calculations indicate that the striped antiferromagnetic state is the ground state as long as the pressure is less than 15 GPa, about 16% compression of volume, then the spin-polarization disappears. It is found that ferromagnetic state is unstable under a large range of pressure. The checkerboard antiferromagnetic order is always higher in total energy due to the smaller calculated magnetic moment, which results in smaller magnetic exchange energy. It also could not give reasonable lattice parameters, for example, to predict smaller c/a ratio and z_{As} . As the volume is compressed by 8%, the corresponding magnetic moment of the checkerboard antiferromagnetic order state decrease from $1.6 \mu_B$ to $0.5 \mu_B$. After having tried several other antiferromagnetic configurations, we find that the striped antiferromagnetic state is the most stable due to its largest magnetic moment. Some of other configurations even could not converge to magnetic solutions.

The high pressure experiment indicates that superconductivity appears at about 2.5 GPa, then T_c reaches a maximum near 3.5 GPa, and disappears above 5.6 GPa¹⁴. As shown in Fig. 4(b), the compression of volume could be estimated to cover such a range of pressure. In terms of the antiferromagnetic results, as volume is compressed from 2% to 8%, the pressure range relevant to superconducting dome is covered completely, while in the non-magnetic calculation, the volume needs to be compressed more, from 4% to 10%.

It is clear that Fe-As bond length is enhanced significantly than Fe-Fe after considering the spin-polarization. Hence, As atom goes away from Fe layer giving a larger z_{As} . With a 10% compression of volume, the magnetic moment of iron decreases from $1.8 \mu_B$ to $1.2 \mu_B$, which reduces the discrepancy of Fe-As bond length between nonmagnetic and antiferromagnetic states. In contrast to tendency of iron related bonding, Ba-As bond length becomes shorter after considering the spin-polarization. In the striped antiferromagnetic state, chemical bonding becomes more rigid against pressure, therefore c/a ratio changes less than nonmagnetic state, as a result, the compressibility is less anisotropic.

Although the Fe-Fe bond length and Fe-As bond length decrease significantly with the increase of pressure, the As-Fe-As bond angles ε change slightly. Under 10% compression of volume, three As-Fe-As angles of antiferromagnetic lattice are found to be 107.6° , 108.3° and 112.5° , roughly changed one degree compared to the ambient condition. Former two values correspond to the As-Fe-As angles whose two As atoms separated by the iron plane, and the latter one represents two As atoms on the same side. Due to the stronger Fe-As bonding in the antiferromagnetic state, the $FeAs_4$ tetrahedra gets more elongated along c -axis, so that $FeAs_4$ tetrahedra in the antiferromagnetic state is distorted less than that in nonmagnetic state, but it is still far away from the ideal structure.

In Fig. 5 we show the band structures and Fermi surfaces with 2%, 4%, 6%, 8% and 10% compression of volume. We can find that the Fermi surfaces expand significantly due to the expansion of band width by pressure. As volume compressed to 4%, corresponding to 3.1 GPa pressure where superconductivity has been observed, the Fermi surfaces lie on antinodal directions of Γ - $Y1$ line expand and across Γ - M line to invade neighbor quarters of BZ. Thus, when pressure increases to 2.5 GPa where the superconductivity takes place, the main change of Fermi surfaces of the striped antiferromagnetic state is to expand in BZ. Furthermore, as volume compressed over 8%, the Fermi surfaces centered around Z point across Γ point to form a connected cylindrical tube. The topological change of Fermi surfaces should respond to the slope change of c/a ratio about 8% compression of volume (see Fig. 4). It is notable that the superconductivity disappears as pressure is higher than 6 GPa, that is roughly same with the place where the Fermi surfaces topological transition occurs.

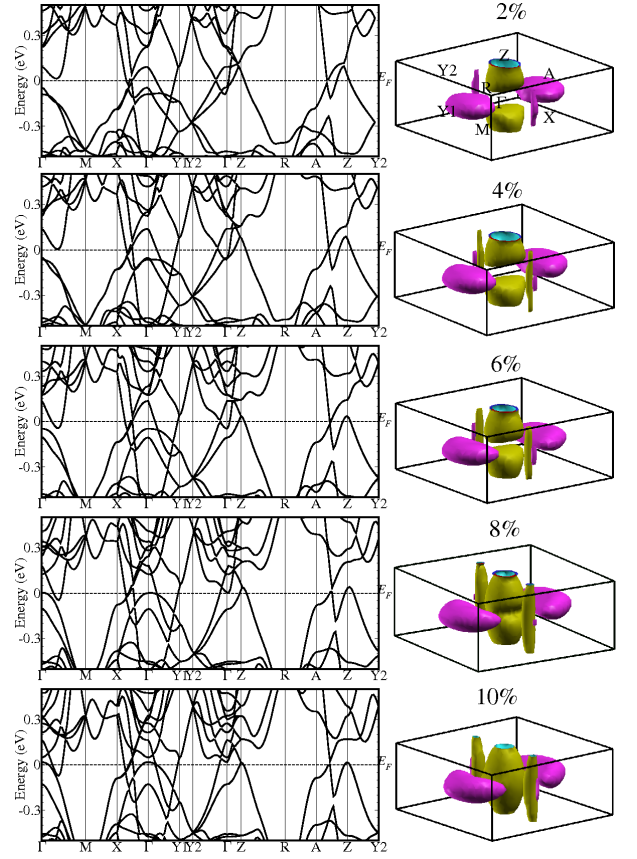


FIG. 5: (color online). Band structures (left column) and Fermi surfaces (right column) of the striped antiferromagnetic state with 2%, 4%, 6%, 8% and 10% (from top to bottom) compression of volume. The 4%, 6%, 8% and 10% corresponds to pressures: 1.7 GPa, 3.1 GPa, 4.7 GPa, 6.4 GPa, and 8.3 GPa, respectively.

However, it is necessary to point out that the shape of the Fermi surfaces is dependent on the magnetic moment which is sensitive to the exchange-correlation potential (LSDA or GGA) and the Fe-As bond length, and thus different calculations give quite different Fermi surfaces. Especially, the closed Fermi surfaces in the Γ - Y line, which are mainly d_{xy} character, seem not to be a common feature of the iron-based superconducting family. The cylinder tubes (see Fig. 5), which are mainly $d_{xz/yz}$ character and show two-dimensional behavior under pressure, are the common features of the iron-based superconducting family. Although the topological transition is observed under the pressure, such a transition is sensitively dependent on the amplitude of magnetic moment. As shown in Fig. 4, the two-dimensional cylinder tube in the Γ - Z line appears when the moment is about $1.3 \mu_B$ in the GGA calculation. Considering that the experimentally observed magnetic moment is only about $0.8 \mu_B$, the cylinder-tube Fermi surfaces of the striped antiferromagnetic state should appear at smaller pressure, because the current electronic structure calculations always overestimate the magnetic moment but describe the

structural parameter very well. It should give some clues for the relationship between magnetism and superconductivity, as discussed previously for LaFeAsO system.⁴

Finally, we investigate pressure effect on the band structures of the nonmagnetic state. As discussed above, the Fe-As bond length is always underestimated in the optimized structure of nonmagnetic state under pressure, consequently d_{xy} bands are below Fermi level at Γ point (See Fig. 1), only shift downwards a little with increasing pressure. While $d_{xz,yz}$ bands shift downwards significantly under pressure, which across Fermi level as compression of volume over 8%, corresponding to a pressure value of 4.7 GPa in nonmagnetic calculations. Such a crossover will lead to a Fermi surface topological transition of the hole-type cylinder-tube closed at Γ point. However, it should be mentioned that the nonmagnetic results might not be true. Because ARPES experiments always indicate the hole-type Fermi surfaces around Γ connects with larger gap in the iron-pnictide materials family, which should be important to superconductivity^{25,26}. Thus the topological transition induced by pressure predicted by nonmagnetic calculation would not coincide with the fact that T_c reach maximum nearby such a pressure.

It has been observed that the superconducting states coexist with the striped magnetic state³⁰, but at present we cannot say that the mechanism of the superconductivity is based on the magnetism. It is just believed that the superconductivity in the Fe based materials is unlikely mediated by phonons, but likely originated from some magnetic or spin fluctuations. Our calculated results indicate that the GGA calculations yield reasonable lattice constants and z_{As} only when we consider the magnetism. This implies that the magnetic effect is essential in these materials. Since the $d_{xz,yz}$ bands around Fermi level are determined by the Fe-As antibonding, as the distance of Fe-As increases, the k_z related hoppings are weakened and the bands become narrow, the large experimental z_{As} parameter leads to typical two-dimensional properties. In current *ab initio* electron-phonon calculations, the optimized structure of nonmagnetic state is used, which results in the underestimation of the Fe-As bond length and more three-dimensional character of Fermi surfaces, that would influence properties of phonon and electron-phonon interaction. Such a magnetism related effect might have substantial influence on the electron-phonon coupling. A calculation including the magnetic effect are highly expected to investigate how much the magnetic background influences the electron-phonon interaction, to reveal the possibility of that phonon might play some important role on the superconductivity. On the other hand, LDA calculations yield smaller magnetic moment and underestimates the z_{As} parameter. The corresponding Fermi surfaces is substantially different from that of ARPES experiments²⁰. If the superconductivity is not directly dependent on the static moment, but determined by the lattice parameters and spin fluctuations, the changing of the moment value does not affect

the superconductivity.

V. COMPARED WITH EXPERIMENTAL RESULTS INVOLVED

The main implication of pressure effect on the crystal structure of BaFe₂As₂ is to shorten the Fe-Fe bond length and the Fe-As bond length, but to maintain As-Fe-As bond angles simultaneously. We could compare the pressure effect on crystal structure with the doping effect in (Ba_{1-x}K_x)Fe₂As₂⁷. With the doping of K into BaFe₂As₂, T_c goes up and reaches a maximum of 38 K at $x=0.4$. The impressive change is that As-Fe-As angle ε becomes the ideal tetrahedral angle of 109.5° as $x=0.4$. Under pressure, the FeAs₄ - tetrahedra is hard to be changed and still far away from the ideal structure. It seems to imply that superconductivity could not be improved simply by hydrostatic pressure in BaFe₂As₂.

In the iron-pnictide superconducting family, the crystal structure, magnetism and superconductivity play complex game. It has been reported that a structural transition of c -axis collapse occurs in CaFe₂As₂^{27,28} under pressure. Such a structural phase transition happens nearby the upper boundary of superconducting dome. In the striped antiferromagnetic calculations of BaFe₂As₂, we find a collapse of c -axis as the compression of volume above 8%, which should be relevant to the topological transition of Fermi surfaces. As the topological transition of Fermi surfaces influence the magnetic moment of iron slightly, the related c/a collapse should not be relative to a magnetic transition. In fact, we observe a magnetic collapse accompanying by a sudden softness of c/a ratio as lattice volume is compressed over 16%, corresponding to near 15 GPa pressure. It is far away from the known superconducting dome (2-6 GPa) up to date. We have performed LSDA calculations to examine the influence of overestimated magnetic moment by GGA. We found that the LSDA calculated magnetic moment is about 0.35 μ_B smaller than GGA, and the magnetic collapse happens at about 14% compression of volume, corresponding to pressure about 13 GPa. These results are consistent with recent experimental report that a suppression of magnetic order by pressure is observed as pressure above about 13 GPa²⁹.

Now, we attempt to consider the implication of the striped antiferromagnetic and nonmagnetic calculations for paramagnetic state. It has been found experimentally that superconductivity coexist with static magnetic order under pressure for BaFe₂As₂³⁰, so that a strong magnetic background is essential to superconductivity in these families. First of all, in order to describe chemical bonding more accurately, the magnetic effect should be considered. Since ferromagnetism is not stable under a large range of pressure, only antiferromagnetic calculations is possible. As the optimized internal parameter z_{As} of the striped antiferromagnetic state is in good agreement with experiments, it might be reasonable to use

these parameters to describe the crystal structures and electronic structures in paramagnetic state than those nonmagnetic results. It coincides with the fact that no significant structural transformation is observed as system goes from antiferromagnetic state to superconducting state or paramagnetic state, except the compression of b/a orthorhombic transition induced by the antiferromagnetic interaction. If the optimized lattice parameters obtained from the striped antiferromagnetic calculations are adopted, it turn out that d_{xz} , d_{yz} and d_{xy} bands always cross Fermi level except for shifting downwards a little under pressure. For such a treatment of paramagnetic state, we found that the energy splitting between $d_{xz,yz}$ and d_{xy} bands decreases from 0.06 eV to 0.04 eV at Γ point as volume is compressed 6%, which indicates that the d_{xy} bands are determined by direct Fe-Fe d_{xy} interaction while the $d_{xz,yz}$ bands are mainly determined by Fe $d_{xz,yz}$ - As $p_{x/y}$ interactions. Nevertheless, the band shapes are maintained under pressure, and the Fermi surfaces are quite similar to those calculations with experimental lattice parameters (see Fermi surfaces of left column in Fig. 1), except the sheets around Γ point expand more. Thus the Fermi surfaces are robust against the pressure, no topological transition is found as the lattice volume compressed up to at least 10%. The impressive features is very different from those nonmagnetic calculations.

It should be reminded that the band structures near Fermi level, as well as Fermi surfaces are sensitive to Fe-As bond length and As-Fe-As angle, which highly depend on the details of the spin-polarization. Our calculations indicate that the shape of bands and Fermi surfaces are almost decided by the value of large range magnetic moment. Therefore, if the pressure induces a high spin polarized state transform to a low spin state (even nonmagnetic state), not only d_{xy} bands shift down to cross Fermi level, but also $d_{xz,yz}$ bands cross Fermi level. This would certainly influence the coupling between different Fermi surfaces, then strongly influence the electronic properties. It would be very interesting to examine the detail of magnetism under pressure by experiment furthermore.

VI. CONCLUSION

In summary, we have employed an accurate all-electronic full-potential linearized augmented plane wave method within the density-functional theory to investigate the effect of pressure on the crystal structure and electronic properties of BaFe_2As_2 . The calculated lattice parameters of the striped antiferromagnetic state is in good agreement with experiment, while nonmagnetic state calculation underestimates c -axis and Fe-As bond lengths and yields a smaller z_{As} . We find that the c -axis is compressed more easily than a -axis in nonmagnetic calculation, while the antiferromagnetic state calculation lead to a nearly isotropic compressibility with pressure up to 6 GPa. With increasing pressure, the FeAs_4 tetrahedra changes little. For the striped antiferromagnetic state, we find that the Fermi surfaces get closer and closer to the Γ point in the $\pm z$ directions when pressure increases from 2 GPa to 6 GPa, corresponding to the pressure region where superconductivity occurs. We observe a Fermi surface topological transition around Γ point as the pressure beyond 6 GPa. The transition should correspond to a small c -axis collapse. A magnetic collapse inducing the softening of c -axis is found when pressure reaches 13 GPa. These first-principles results should be useful to understanding the antiferromagnetism and electronic states in the FeAs-based materials, and may have some useful implications to the superconductivity.

Acknowledgments

This work is supported by Nature Science Foundation of China (Grant Nos. 10704024, 10774180, and 10874232), by Shanghai Rising-Star Program (Grant No. 08QA14026), and by the Chinese Academy of Sciences (Grant No. KJCX2.YW.W09-5).

-
- ¹ Y. Kamihara, T. Watanabe, M. Hirano, and H. Hosono, J. Am. Chem. Soc. **130**, 3296 (2008).
 - ² I. I. Mazin, D. J. Singh, M. D. Johannes, and M. H. Du, Phys. Rev. Lett. **101**, 057003 (2008).
 - ³ D. J. Singh and M. H. Du, Phys. Rev. Lett. **100**, 237003 (2008).
 - ⁴ Z. P. Yin, S. Lebegue, M. J. Han, B. P. Neal, S. Y. Savrasov, and W. E. Pickett, Phys. Rev. Lett. **101**, 047001 (2008).
 - ⁵ Z. A. Ren, W. Lu, J. Yang, W. Yi, X. L. Shen, Z. C. Li, G. C. Che, X. L. Dong, L. L. Sun, F. Zhou, and Z. X. Zhao, Chin. Phys. Lett. **25**, 2215 (2008).
 - ⁶ C. Wang, L. Li, S. Chi, Z. Zhu, Z. Ren, Y. Li, Y. Wang, X. Lin, Y. Luo, S. Jiang, X. Xu, G. Cao, and Z. Xu, Europhysics Letters **83**, 67006 (2008), arXiv:0804.4290 (2008).

- ⁷ M. Rotter, M. Tegel, and D. Johrendt, Phys. Rev. Lett. **101**, 107006 (2008), arXiv:0805.4630 (2008).
- ⁸ M. Rotter, M. Pangerl, M. Tegel, and D. Johrendt, Angew. Chem. Int. Ed. **47**, 7949 (2008), arXiv:0807.4096 (2008).
- ⁹ C. de la Cruz, Q. Huang, J. W. Lynn, J. Li, W. Ratcliff II, J. L. Zarestky, H. A. Mook, G. F. Chen, J. L. Luo, N. L. Wang, and P. Dai, Nature **453**, 899 (2008), arXiv:0804.0795 (2008).
- ¹⁰ L. Boeri, O. V. Dolgov, and A. A. Golubov, Phys. Rev. Lett. **101**, 026403 (2008).
- ¹¹ I. I. Mazin, M. D. Johannes, L. Boeri, K. Koepernik, and D. J. Singh, Phys. Rev. B **78**, 085104 (2008), arXiv:0806.1869 (2008).
- ¹² M. Rotter, M. Tegel, D. Johrendt, I. Schellenberg, W. Hermes, and R. Pottgen, Phys. Rev. B **78**, 020503(R) (2008),

- arXiv:0805.4021 (2008).
- ¹³ Q. Huang, Y. Qiu, Wei Bao, M.A. Green, J.W. Lynn, Y.C. Gasparovic, T. Wu, G. Wu, and X.H. Chen, *Phys. Rev. Lett.* **101**, 257003 (2008), arXiv:0806.2776 (2008).
 - ¹⁴ P. L. Alireza, J. Gillett, Y. T. Chris Ko, S. E. Sebastian, and G. G. Lonzarich, *J. Phys.: Condens. Matter* **21**, 012208 (2008), arXiv:0807.1896 (2008).
 - ¹⁵ M. S. Torikachvili, S. L. Budko, N. Ni, and P. C. Canfield, *Phys. Rev. Lett.* **101**, 057006 (2008).
 - ¹⁶ P. Blaha, K. Schwarz, G. K. H. Madsen, D. Kvasnicka, and J. Luitz, WIEN2k, An Augmented Plane Wave+Local Orbitals Program for Calculating Crystal Properties (Technical University Wien, Austria, 2001), ISBN3-9501031-1-2.
 - ¹⁷ J. P. Perdew and Y. Wang, *Phys. Rev. B* **45**, 13244 (1992).
 - ¹⁸ J. P. Perdew, K. Burke, and M. Ernzerhof, *Phys. Rev. Lett.* **77**, 3865 (1996).
 - ¹⁹ Y. Su, P. Link, A. Schneidewind, T. Wolf, Y. Xiao, R. Mitral, M. Rotter, D. Johrendt, T. Brueckel, and M. Loewenhaupt, arXiv:0807.1743 (2008).
 - ²⁰ L. X. Yang, H. W. Ou, J. F. Zhao, Y. Zhang, D. W. Shen, B. Zhou, J. Wei, F. Chen, M. Xu, C. He, X. F. Wang, T. Wu, G. Wu, Y. Chen, X. H. Chen, Z. D. Wang, and D. L. Feng, arXiv:0806.2627 (2008).
 - ²¹ F. Ma, Z. Y. Lu, and T. Xiang, arXiv:0806.3526 (2008).
 - ²² G. Xu, H. Zhang, X. Dai, and Z. Fang, arXiv:0807.1401 (2008).
 - ²³ D. J. Singh, *Phys. Rev. B* **78**, 094511 (2008), arXiv:0807.2643 (2008).
 - ²⁴ I. A. Nekrasov, Z. V. Pchelkina, and M. V. Sadovskii, *JETP Letters* **88**, 144 (2008), arXiv:0806.2630 (2008).
 - ²⁵ H. Ding, P. Richard, K. Nakayama, T. Sugawara, T. Arakane, Y. Sekiba, A. Takayama, S. Souma, T. Sato, T. Takahashi, Z. Wang, X. Dai, Z. Fang, G. F. Chen, J. L. Luo, and N. L. Wang, *Europhysics Letters* **83**, 47001 (2008), arXiv:0807.0419 (2008).
 - ²⁶ L. Zhao, H. Liu, W. Zhang, J. Meng, X. Jia, G. Liu, X. Dong, G. F. Chen, J. L. Luo, N. L. Wang, G. Wang, Y. Zhou, Y. Zhu, X. Wang, Z. X. Zhao, Z. Y. Xu, C. T. Chen, and X. J. Zhou, *Chin. Phys. Lett.* **25**, 4402 (2008), arXiv:0807.0398 (2008).
 - ²⁷ A. Kreyssig, M. A. Green, Y. Lee, G. D. Samolyuk, P. Zajdel, J. W. Lynn, S. L. Bud'ko, M. S. Torikachvili, N. Ni, S. Nandi, J. B. Leão, S. J. Poulton, D. N. Argyriou, B. N. Harmon, R. J. McQueeney, P. C. Canfield, and A. I. Goldman, *Phys. Rev. B* **78**, 184517 (2008), arXiv:0807.3032 (2008).
 - ²⁸ T. Yildirim, *Phys. Rev. Lett.* **101**, 057010 (2008), arXiv:0804.2252 (2008).
 - ²⁹ H. Fukazawa, N. Takeshita, T. Yamazaki, K. Kondo, K. Hirayama, Y. Kohori, K. Miyazawa, H. Kito, H. Eisaki, and A. Iyo, *J. Phys. Soc. Jpn.* **77**, 105004 (2008), arXiv:0808.0718 (2008).
 - ³⁰ T. Goko, A. A. Aczel, E. Baggio-Saitovitch, S. L. Bud'ko, P. C. Canfield, J. P. Carlo, G. F. Chen, P. C. Dai, A. C. Hamann, W. Z. Hu, H. Kageyama, G. M. Luke, J. L. Luo, B. Nachumi, N. Ni, D. Reznik, D. R. Sanchez-Candela, A. T. Savici, K. J. Sikes, N. L. Wang, C. R. Wiebe, T. J. Williams, T. Yamamoto, W. Yu, and Y. J. Uemura, arXiv:0808.1425 (2008).